Supporting Information for "Suspended-sediment induced stratification inferred from concentration and velocity profile measurements in the lower Yellow River, China"

Andrew J. Moodie[1], Jeffrey A. Nittrouer[1], Hongbo Ma[1], Brandee N. Carlson[1], Wang, Yuanjian[2], Michael P. Lamb[3], and Gary Parker[4,5]

[1]Department of Earth, Environmental and Planetary Sciences, Rice University, Houston, Texas, USA

[2]Yellow River Institute of Hydraulic Research, Zhengzhou, Henan 450000, China

[3]Division of Geological and Planetary Sciences, California Institute of Technology, Pasadena, California, USA

[4]Department of Civil and Environmental Engineering, University of Illinois at Urbana-Champaign, Champaign, Illinois, USA

[5]Department of Geology, University of Illinois at Urbana-Champaign, Champaign, Illinois, USA

Contents of this file

1. Yellow River station survey dataset

The surveys in this study generated a total of 54 stations, where concentration profiles were measured and modeled. Figure S1 depicts each of these stations graphically. Velocity profiles were measured in only 16 stations (Figure S2). The station data are included as part of the Yellow River Kenli Station Survey Dataset (available from Zenodo 10.5281/zenodo.3457639).

Figure S3 depicts the fraction of samples from each station that were below 15 μm, and excluded from the analysis in the main text.

2. Shear velocity calibration

Velocity profile data were not collected in the 2015 survey, and so a relationship for flow depth and shear velocity was initially substituted (i.e., depth slope product, $u_* = \sqrt{gHS_0}$; Leopold et al., 1995). However, the only varying parameter in the depth-slope product calculations is the flow depth (H), and local variability in flow depth is poorly correlated to reach-averaged shear stress and suspended sediment concentration (e.g., An et al., 2018, Figure 6).

In 2016 and 2018, water velocity profile measurements were made at each station with an acoustic Doppler current profiler (ADCP) and a mechanical propeller-driven velocimeter. Local shear velocity was determined by combining depth-averaged velocity derived from ADCP and velocimeter measurements with a resistance relation (Engelund & Hansen, 1967; Ma et al., in review). To estimate shear velocity when no direct velocity measurements are available, we produce a calibration that relates water discharge data (collected $\sim$10 km upstream at a nearby gauging station operated by the Yellow River Hydrological Bureau) and the local flow depth to reach-scale shear velocity. The calibration is determined by linear regression in log-transformed space ($R^2 = 0.80$; e.g., Trampush et al., 2014):

$$\log_{10} u_* = b_0 + b_1 \log_{10} Q_w + b_2 \log_{10} H. \tag{1}$$

Taking the logarithm of dimensional variables (shear velocity, discharge, and depth have units of m/s, m^3/s, and m, respectively) implicitly ratios the variables of interest to the relevant unit-dimension (e.g., 0.05 m/s / 1 m/s), such that all variables of the linear regression are dimensionless. Following the determination of the regression parameters in log-transformed space, the parameters are rescaled to a power-law calibration with dimensional quantities (Figure 6):

$$u_{*,\text{calib}} = 0.0202[Q_w]^{0.083}[H]^{0.298}. \tag{2}$$

Note, that Equation 13 is non-homogeneous, and should not be applied beyond the purposes of this calibration. For consistency, this calibration is applied to determine the shear velocity for all survey stations. The effects of form drag on shear stress partitioning, including bedforms (McLean, 1991, 1992; McLean et al., 1994), are ignored in calibrating the shear velocity.

Figure S4 shows the difference between the calibrated shear velocity and a standard depth-slope product prediction, which depends only on depth, because slope is fixed in the calculations.

3. Buoyancy-stratified simulations for global rivers dataset

Concentration profiles were simulated for bankfull flow conditions for all rivers in the global compilation from (main text Figure 13; Li et al., 2015). A single grain size (D_{50}), normal flow, and the entrainment relation from (Wright & Parker, 2004) is assumed for the simulations.

Additional simulations randomly sample the parameter space delineated by this global rivers dataset, and evaluate the depth-averaged eddy viscosity reduction (Figure S5a). This exhaustive parameter space search demonstrates grain-size dependent density stratification, and that the (Wright & Parker, 2004) α relation (main text, Equation 10) covers the region of highest density of simulation results (Figure S5b).

4. Grain size and concentration of overbank / diverted sediment

Density stratification alters the grain-size distribution and concentration of sediment in the water column. In the Yellow River measurements, the overall sediment concentration is reduced by 1–20% in the upper 20% of the flow, compared to predictions by the dilute-suspension model. The concentrations of the coarsest grain-size classes ($\geq 208\mu$m) are increased relative to the dilute-suspension prediction (Figure S6). In contrast, concentrations of medial grain sizes (73–208μm, which comprise most of the grain-size distribution) are reduced relative to the prediction, and the finest grain-size classes concentrations ($< 73\mu$m) are relatively unaffected. This suggests that the increase in the coarsest grain-size classes leads to the net increase in suspended sediment flux, due to stratification.

Additionally, the grain-size distribution is finer, according to a Wilcoxon signed rank test (Figure S7). The change is grain-size distribution is subtle, despite the significant reduction in overall grain size. The grain-size distribution change may be larger for rivers with coarser material.

References

An, C., Moodie, A. J., Ma, H., Fu, X., Zhang, Y., Naito, K., & Parker, G. (2018). Morphodynamic model of lower Yellow River: flux or entrainment form for sediment mass conservation? *Earth Surface Dynamics*, *6*(4), 989–1010. doi: 10.5194/esurf-6-989-2018

Engelund, F., & Hansen, E. (1967). *A monograph on sediment transport in alluvial streams*. Technisk Vorlag, Copenhagen, Denmark.

Leopold, L. B., Wolman, M. G., & Miller, J. P. (1995). *Fluvial processes in geomorphology* (Dover ed ed.). New York: Dover Publications.

Li, C., Czapiga, M. J., Eke, E. C., Viparelli, E., & Parker, G. (2015, January). Variable Shields number model for river bankfull geometry: bankfull shear velocity is viscosity-dependent but grain size-independent. *Journal of Hydraulic Research*, *53*(1), 36–48. doi: 10.1080/00221686.2014.939113

Ma, H., Nittrouer, J. A., Fu, X., Parker, G., Zhang, Y., Wang, Y., ... Cisneros, J. (in review). Amplification of downstream flood stage due to damming of fine-grained rivers. *Science Advances*.

McLean, S. R. (1991, November). Depth-Integrated Suspended-Load Calculations. *Journal of Hydraulic Engineering*, *117*(11), 1440–1458. doi: 10.1061/(ASCE)0733-9429(1991)117:11(1440)

McLean, S. R. (1992). On the calculation of suspended load for noncohesive sediments. *Journal of Geophysical Research*, *97*(C4), 5759. doi: 10.1029/91JC02933

McLean, S. R., Nelson, J. M., & Wolfe, S. R. (1994). Turbulence structure over two-dimensional bed forms: Implications for sediment transport. *Journal of Geophysical Research*, *99*(C6), 12729. doi: 10.1029/94JC00571

Trampush, S. M., Huzurbazar, S., & McElroy, B. (2014). Empirical assessment of theory for bankfull characteristics of alluvial channels. *Water Resources Research*, *50*(12), 9211-9220. doi: 10.1002/2014WR015597

Wright, S., & Parker, G. (2004, August). Flow Resistance and Suspended Load in Sand-Bed Rivers: Simplified Stratification Model. *Journal of Hydraulic Engineering*, *130*(8), 796–805. doi: 10.1061/(ASCE)0733-9429(2004)130:8(796)

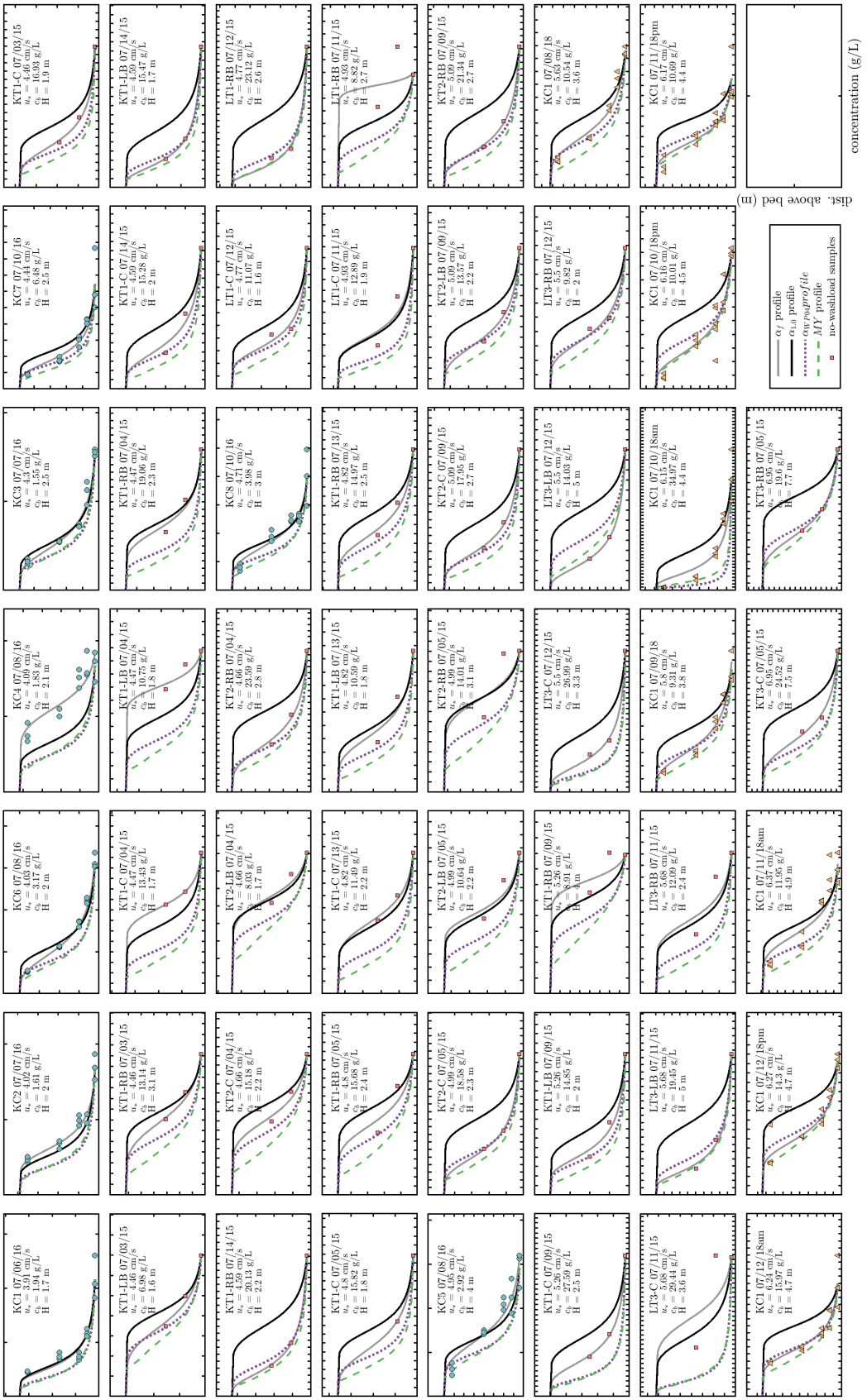

Figure S1. Yellow River measured and modeled concentration profiles.

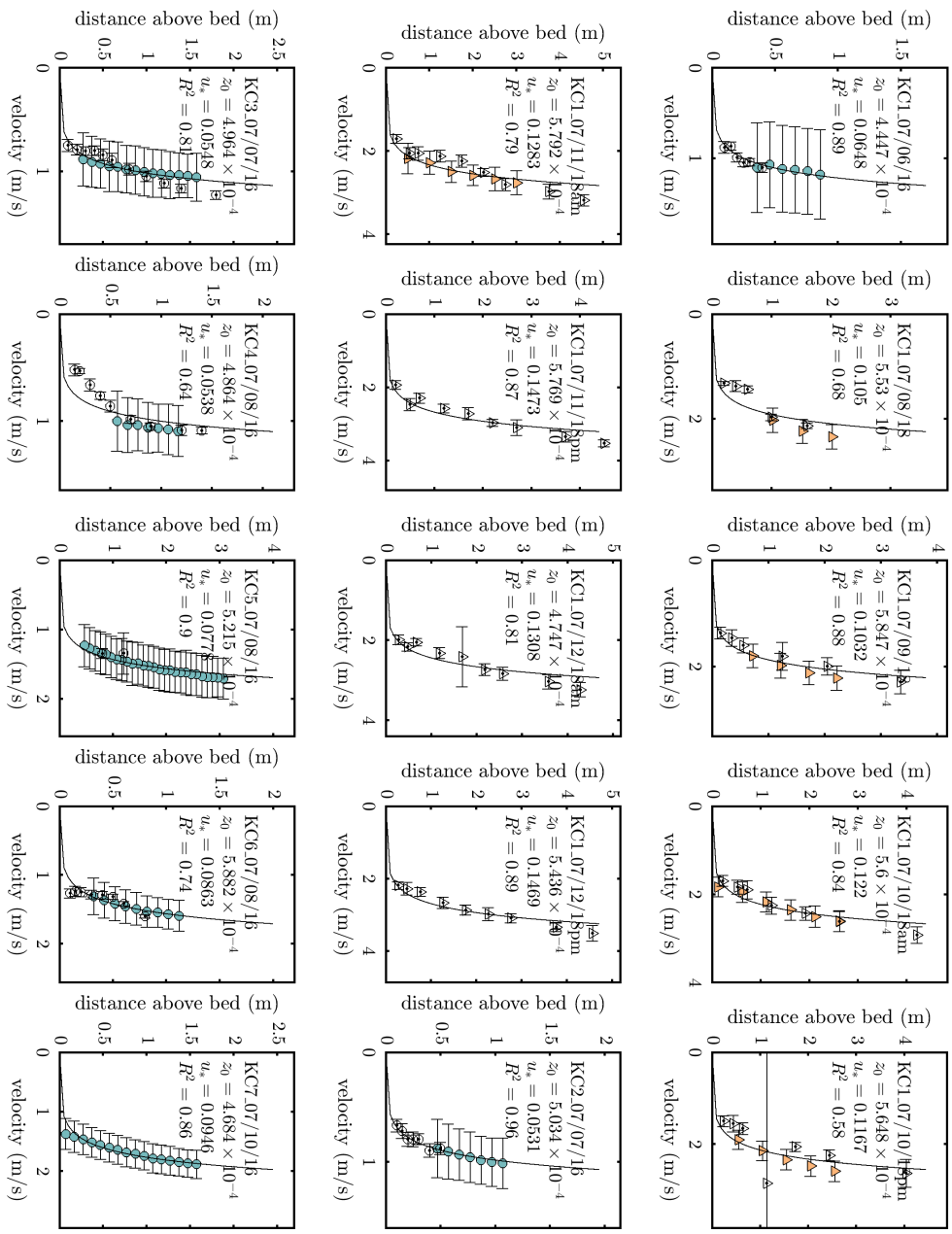

Figure S2. Yellow River measured and modeled velocity profiles.

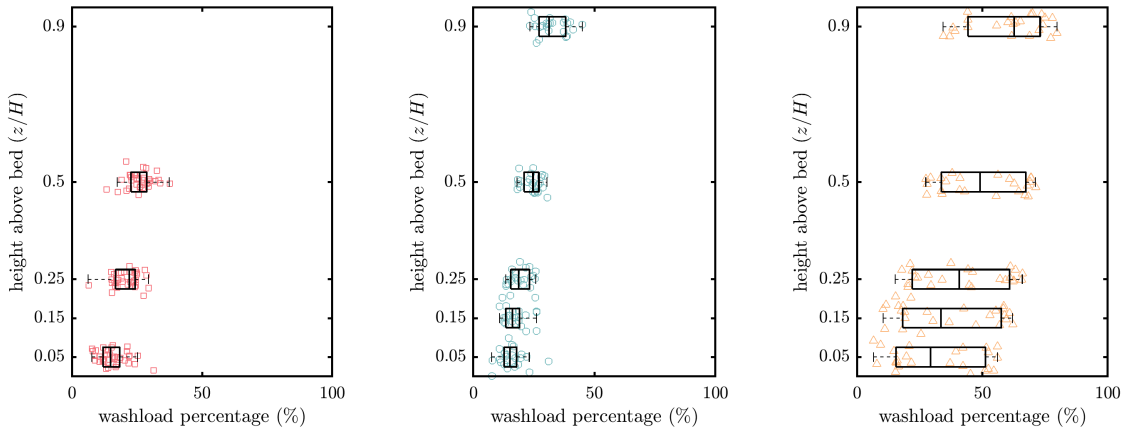

Figure S3. Fraction of samples finer than $< 15\mu$m, separated by survey year and normalized height above the bed.

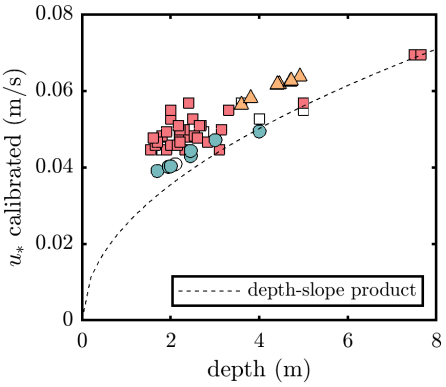

Figure S4. a) Difference between the calibrated shear velocity and a standard depth-slope product prediction depending only on depth (slope is fixed in the calculations).

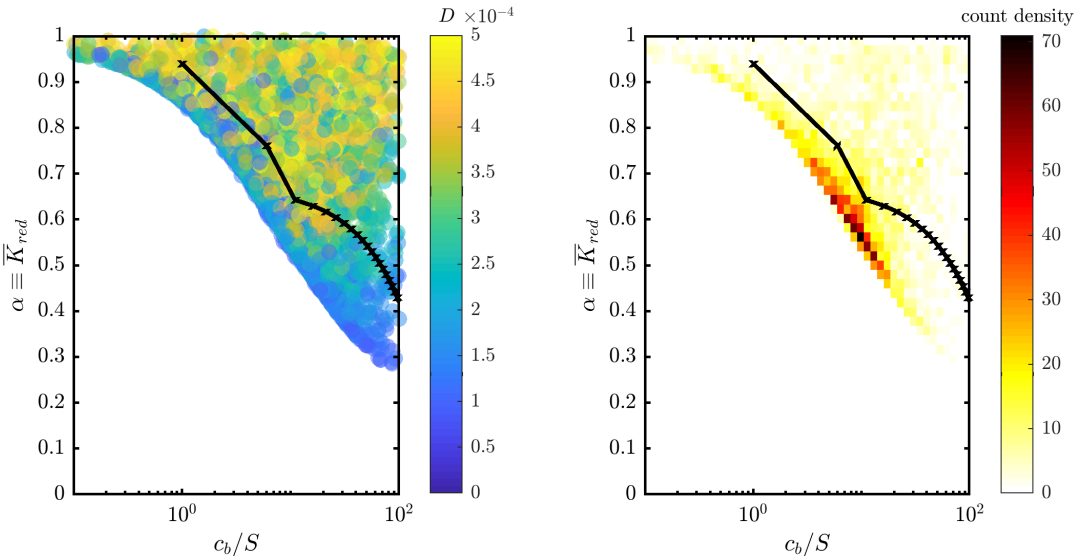

Figure S5. Simulations of the buoyancy stratified model exploring the parameter space defined by the global rivers dataset (Li et al., 2015).

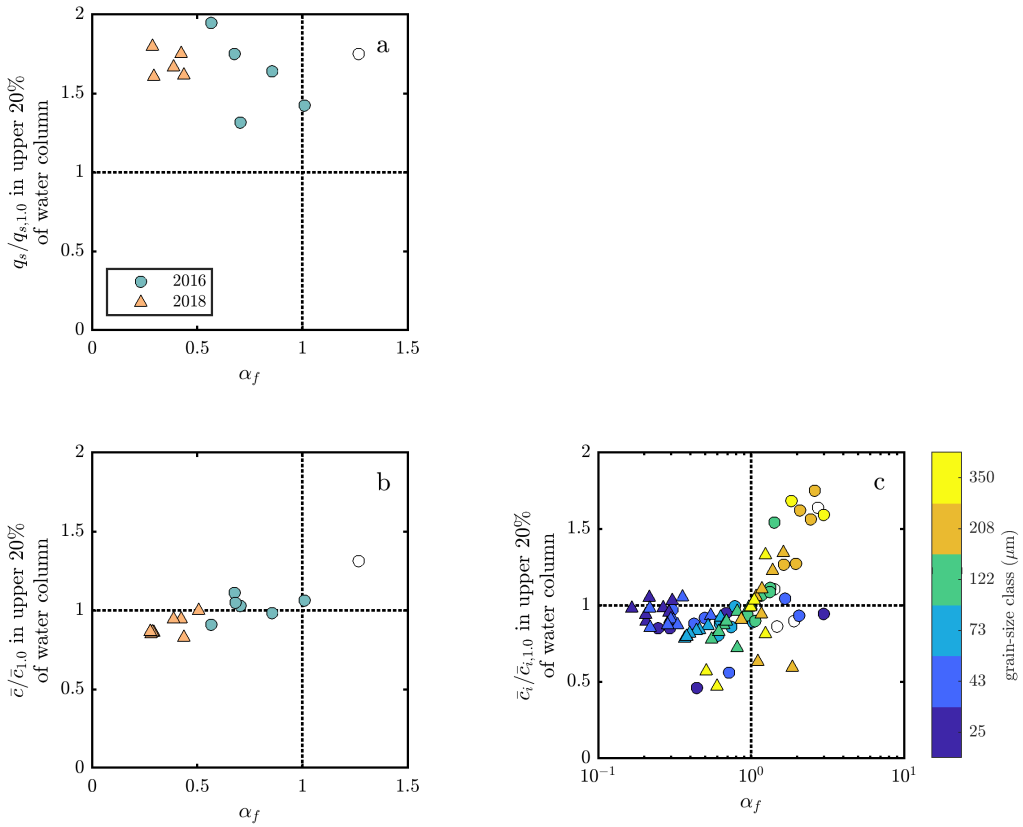

Figure S6. a) Ratio of depth-discharge integrated sediment transport (Equation 1) under density-stratified flow to predicted transport assuming a dilute suspension ($\alpha = 1$ in Equations 4–5) over the upper 20% of the flow depth. b) Ratio of grain-size class cumulative measured concentration in the the upper 20% of the flow depth to predicted concentration assuming a dilute suspension. c) Ratio of grain-size specific measured concentration in the the upper 20% of the flow depth to predicted concentration assuming a dilute suspension.

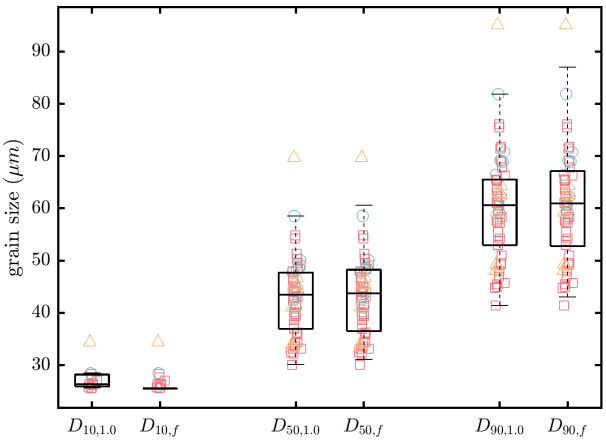

Figure S7. Grain-size distribution D_{10}, D_{50}, and D_{90} of sediment in the upper 20% of the flow for clear-water model (1.0), and concentration profiles fit to the field measurements (f).